JMEPEG (2009) 18:1078–1085
DOI: 10.1007/s11665-009-9353-6

1059-9495/$19.00

Effect of Destabilization Heat Treatments on the Microstructure of High-Chromium Cast Iron: A Microscopy Examination Approach

A.E. Karantzalis, A. Lekatou, and E. Diavati

(Submitted October 8, 2008; in revised form December 18, 2008)

A 18.22 wt.% Cr white iron has been subjected to various destabilization heat treatments. Destabilization at 800 °C caused gradual precipitation of $M_{23}C_6$ secondary carbide particles with time leading to a gradual increase in the bulk hardness. At 900, 1000, and 1100 °C, an initial sharp increase in bulk hardness with time occurred, reaching a plateau that was followed by a slightly decreasing trend. The combination of martensite formed, stoichiometry, and morphology of the secondary carbides present (mostly M_7C_3) are responsible for the obtained values of hardness. At 1100 °C, severe dissolution of the secondary carbides and consequent stabilization of the austenitic phase took place. Maximum hardness values were obtained for destabilization at 1000 °C. The correlation between bulk hardness and microstructural features was elaborated.

Keywords cast iron, destabilization treatment, high chromium, secondary carbides

1. Introduction

The high hardness and the exceptional resistance to abrasion wear have made high-chromium cast irons as the most broadly used materials in mining, metallurgy, and other heavy load transfer applications (Ref 1-3). This attractive behavior is mainly associated with the various phases present in their microstructure. Tabrett and Sare (Ref 1), in their extensive review, address all the key issues that can control and modify the microstructure of these materials. Especially, as far as the relation between microstructure and resistance to abrasion wear is concerned, the reader should address to the works of Tabrett and Sare (Ref 1-3) and Dogan et al. (Ref 4-6).

The as-cast material basically consists of an austenitic matrix and an eutectic mixture of austenite/carbide (M_7C_3). This pristine microstructure can significantly be altered by different critical (destabilization) and subcritical heat treatments. The applied heat treatments have two objectives: (a) The precipitation of secondary carbides and (b) the transformation of the primary austenitic matrix to other phases, most desirably martensite. The destabilization heat treatments are usually conducted at 800-1100 °C, for 1-6 h (Ref 1-10) leading mainly to extensive precipitation of secondary carbides and martensitic transformation of the matrix; they are followed by subcritical heat treatments, usually performed at 200-600 °C, for 2-6 h (Ref 1-10), leading mainly to further precipitation of secondary carbides.

As mentioned above, the role of the destabilization heat treatments is very important. During the process, extensive precipitation of secondary carbides takes place that lead to the austenitic matrix destabilization, due to its depletion of alloying elements and, consequently, its transformation into martensite during cooling (Ref 1-10). Several experimental efforts have been carried out to ascertain the nature, morphology, and mechanisms of secondary carbide precipitation during destabilization heat treatments (Ref 10-20).

Asensio et al. (Ref 10) provide a very useful first approach on the carbide phases (primary and secondary) expected, based on the chemical composition of the as-cast material. Powell and Laird (Ref 11) examined the morphology, structure, and growth sequence of secondary carbides, as a function of the Cr content and the destabilization treatment parameters. They observed that increasing the Cr content, the secondary carbide stoichiometry followed the sequence M_3C, M_7C_3, and $M_{23}C_6$. Their morphology varied from rod like, for M_3C and M_7C_3, to fiber like, for $M_{23}C_6$. In all cases, precipitation of secondary carbides took place within the austenitic grains without any evidence of preferential growth from the eutectic carbides. Wiengmoon et al. (Ref 12) extensively investigated the precipitation and growth sequence of secondary carbides after destabilization heat treatments to 30% Cr cast irons. They observed that, in lack of vanadium additions, the destabilization heat treatments caused massive precipitation of rod-like $M_{23}C_6$ particles within the austenitic dendrites with a cube-cube to the austenitic matrix crystal lattice matching. They, also, noticed a partial transformation of the eutectic M_7C_3 to $M_{23}C_6$. Vanadium additions refined the structure of the eutectic carbide phase, increased its volume fraction, whereas they led to ferritic matrix formation in the as-cast condition. $M_{23}C_6$ secondary carbide precipitation for short periods of destabilization heat treatment (1273 K) has also been reported by Powell and Bee (Ref 13), while dealing with a 18%Cr white cast iron. Prolonged

A.E. Karantzalis, A. Lekatou, and **E. Diavati**, Department of Materials Science and Engineering, Laboratory of Applied Metallurgy, University of Ioannina, University Campus, 45110 Ioannina, Greece. Contact e-mails: karantzalis@hotmail.com, alekatou@cc.uoi.gr.

destabilization periods at the same temperature have resulted in the combined formation of $M_{23}C_6$ and M_7C_3. They have also mentioned the formation of secondary carbide phases at subgrain boundaries, during solidification. Carpenter et al. (Ref 14), while examining the destabilization behavior of a 27%Cr cast iron, identified the nature of the precipitated secondary carbides as that of $M_{23}C_6$, using XRD techniques. Wang et al. (Ref 15) examined the destabilization response of a 16%Cr-1%Mo-1%Cu cast iron. They observed two types of $M_{23}C_6$ secondary carbides: one of cubic morphology with a specific to the matrix orientation and one of grainy morphology with no specific to the matrix orientation; the second was mainly formed during the cooling stage of the destabilization treatment. They also noticed a gradual transformation of $M_{23}C_6$ to M_7C_3 rods after prolonged destabilization. Carpenter and Carpenter (Ref 16) investigated the eutectic carbide stability in relation to the destabilization treatment parameters and observed a behavior analogous to those reported in previous works (Ref 17-19), regarding the M_7C_3 to $M_{23}C_{26}$ transformation. Bedolla-Jacuinde et al. (Ref 20) extensively studied the effect of destabilization treatment parameters on the nature, extent, and morphology of secondary carbide precipitation. In their work, destabilization of a 17%Cr-2%Mo-2%V-1.80%Ni white cast iron was carried out at 900, 1000, and 1150 °C for 5 min up to 8 h. They reported decreasing secondary carbide precipitation with decreasing temperature. They also noted that high temperatures stabilized an austenitic phase free of secondary carbide precipitates. At 900 and 1000 °C, the extent of carbide precipitation increased with time, reaching a maximum; then, it decreased due to either dissolution or coarsening phenomena. In their work, the highest hardness values were obtained after destabilization at 900 °C for 1-2 h; these conditions ensured an optimum combination of martensite and finely dispersed secondary carbide precipitates.

The scope of the present investigation is to further enlighten the effect of time and temperature of destabilization treatment on the secondary carbide precipitation for a white cast iron, by using a wide range of temperatures and times contrary to the afore-mentioned works. The employed alloy is relatively free of other strong carbide forming elements, such as Mo and V.

2. Experimental Procedure

The as-cast high-chromium white iron examined in this work, contains 2.33 wt.% C, 18.22 wt.% Cr, 0.60 wt.% Si, 0.66 wt.% Mn, 0.34 wt.% Mo, 0.31 wt.% Ni, 0.47 wt.% Cu, 0.027 wt.% P, Fe-balanced. The material was prepared by melting the appropriate raw material in an induction furnace. Casting was then performed in bentonite sand molds, at the temperature range of 1440-1460 °C. Specimens were cut off and subjected to destabilization heat treatment at 800, 900, 1000, and 1100 °C for 30, 60, 90, 120, 150, 180, 210, and 240 min.

Specimens were mounted, ground, and polished following standard metallographic procedure and chemically etched by a 10 wt.% ammonium persulfate aqueous solution. Hardness (HRC) was measured by a portable hardness tester (brand Equotip). SEM inspection was carried out using a Zeiss Supra 35VP SEM equipped with a Roentec Quantax (Bruker AXs) EDS system and a JEOL 5600 SEM system equipped with an Oxford Instruments EDS analysis system.

3. Results and Discussion

3.1 Hardness Measurements

Figure 1 shows the effect of the destabilization treatments on the bulk hardness of the alloy. At 800 °C, hardness is almost steadily increasing with time. At the other destabilization

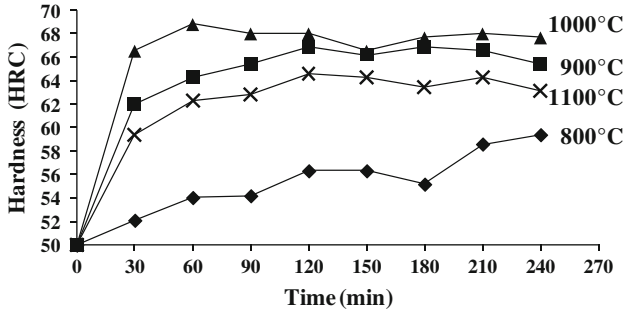

Fig. 1 Bulk hardness vs. time for the different destabilization temperatures

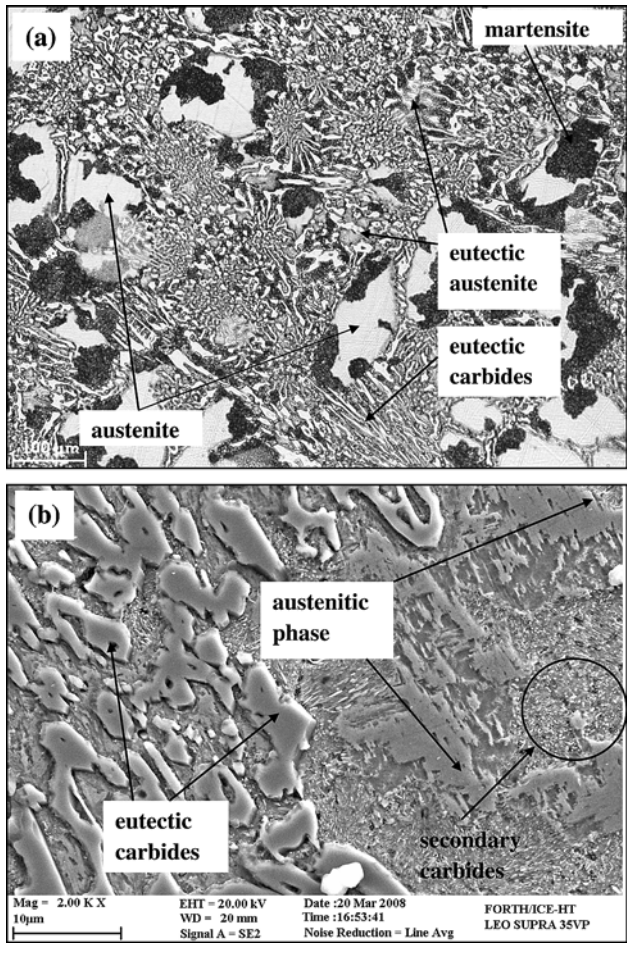

Fig. 2 Destabilization at 800 °C for 30 min. (a) Eutectic carbide particles/austenite and austenitic dendrites partially transformed to martensite. (b) Extensive plate-like secondary carbide precipitation of $M_{23}C_6$ stoichiometry

temperatures, the material exhibits similar behavior: an initial sharp increase in hardness is followed by a gradual increase reaching a plateau after ~2 h. Eventually, a slight decrease in hardness is observed after prolonged destabilization (~3 h). Irrespectively of time, the lowest hardness is attained at 800 °C, whereas the highest hardness is attained at 1000 °C. Comparatively, the hardness values follow the trend 800 < 1100 < 900 < 1000 °C, in increasing order.

3.2 Microstructural Observations

3.2.1 As-Cast Alloy. The microstructure of the as-cast alloy basically consists of metastable austenitic dendrites and an eutectic mixture of austenite/M_7C_3, as reported in a previous work (Ref 21). Often, a thin martensitic layer is formed around the periphery of the eutectic carbide particles, as a result of alloying element's local depletion of the austenitic phase leading to the formation of martensite during cooling. These observations are common in many experimental efforts (Ref 1-8, 21). For further details on the as-cast microstructure, the reader should address to the related references (Ref 1-8, 21).

3.2.2 Effect of Destabilization Temperature on Microstructure. To examine the effect of the destabilization temperature, two different times (for each temperature) were selected: 30 and 180 min.

Figure 2(a) illustrates an optical micrograph of the alloy structure after 30 min at 800 °C, where partial transformation of the austenitic dendrites can be observed. The morphological features of the transformed areas indicate the presence of martensite. Further examination of the transformed/martensitic areas with SEM (Fig. 2b) reveals the existence of fine carbide precipitates of equiaxed morphology. EDX analysis could not produce absolute results on their stoichiometries, owing to their fine size. However, carbide precipitates of similar morphological features have been identified in other experimental efforts as $M_{23}C_6$ (Ref 11, 13).

Further increase in the destabilization temperature to 900 °C has led to extensive transformation of the pre-eutectic austenite to martensite (Fig. 3a). SEM examination (Fig. 3b) of the martensitic islands did reveal a limited precipitation of fine plate-like carbide particles. At the same time, rod-like secondary carbide particles have started to precipitate with stoichiometries most likely of the $M_{23}C_6$ type. EDX analysis of these carbides gave stoichiometries of the M_7C_3 type. This observation is in agreement with other experimental findings (Ref 11-16).

Increase in the destabilization temperature to 1000 °C causes further microstructural changes. Figure 4(a) shows the

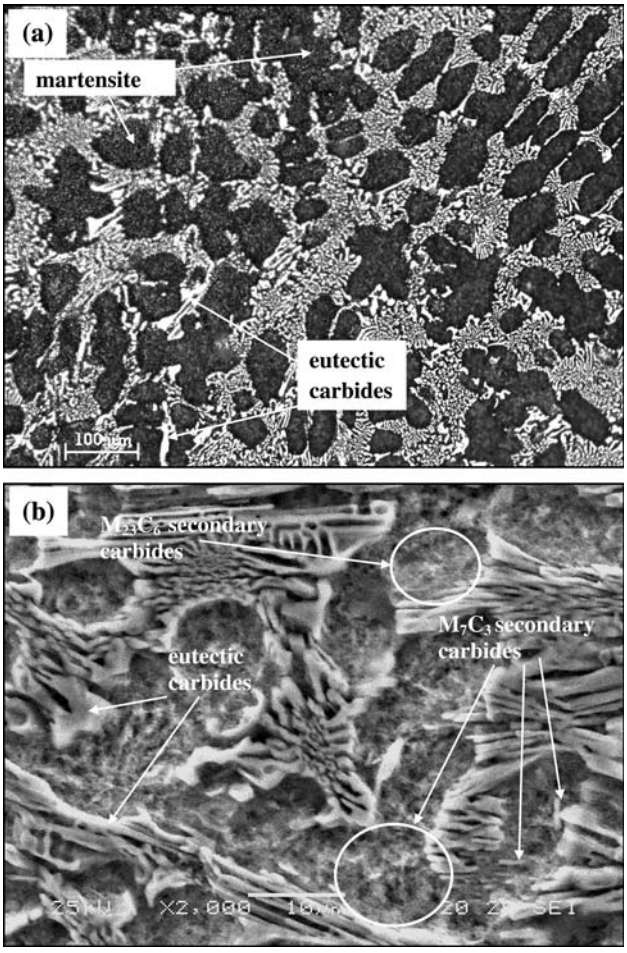

Fig. 3 Destabilization at 900 °C for 30 min. (a) Eutectic carbide particles and martensite. (b) Precipitation of $M_{23}C_6$ secondary carbide platelets and indications of formation of M_7C_3 rods

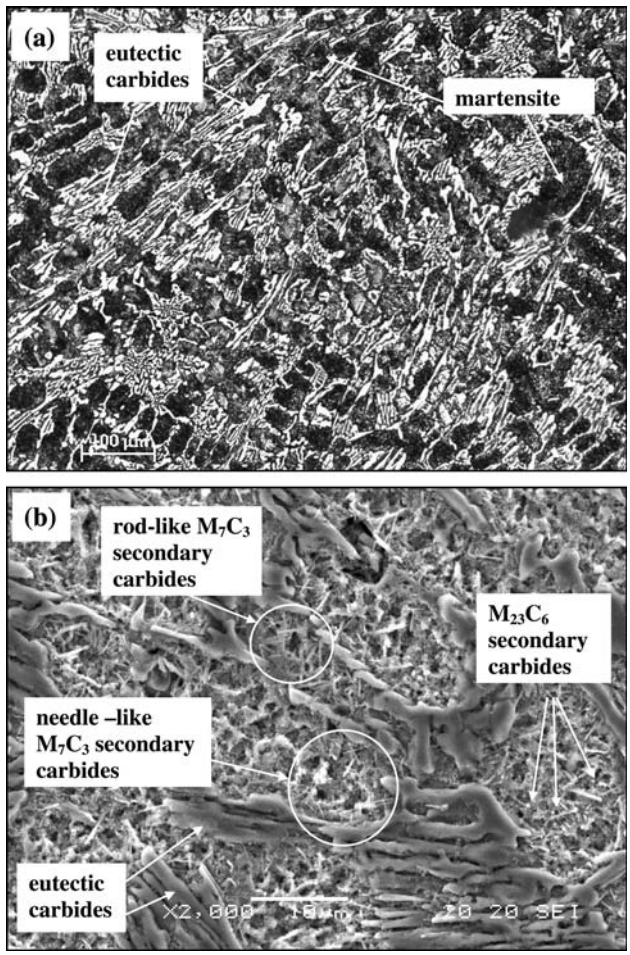

Fig. 4 Destabilization at 1000 °C for 30 min. (a) Eutectic carbide particles and martensite. The brighter contrast of the martensite islands, in comparison with that of Fig. 3, is due to extensive carbide precipitation. (b) Extensive precipitation of needle/rod-like M_7C_3 secondary carbide particles. Some $M_{23}C_6$ secondary carbide platelets are also discerned

microstructure of the specimen after 30 min at 1000 °C. The austenite surrounding the martensite islands is limited, and within the martensitic islands brighter areas are observed. This is an indication of extensive secondary carbide precipitation. Indeed, SEM examination reveals an extensive secondary carbide precipitation within the martensitic areas (Fig. 4b). These carbides are of dual morphology: one of needle-like and one of rod-like morphology. In both cases, the stoichiometry after EDX analysis is of the M_7C_3 type, while no preferential association with the primary carbide phases can be noticed. Precipitation of $M_{23}C_6$ plate-like secondary carbides is also indicated.

Figure 5(a) shows the microstructure of the specimen after 30 min at 1100 °C. Clearly, an increase in the austenitic phase, especially the one involved in the eutectic microconstituent, can be observed. This increase is associated with a dissolution process of the eutectic carbide phases. At the same time, the high amount of alloying elements provided to the austenitic phase, through this dissolution process, has prevented any transformation during cooling. A coarsening effect on the eutectic carbide particles may be seen, as well. Moreover, SEM examination (Fig. 5b) reveals a coarsening effect on the secondary carbide particles, which, to a great extent, maintain their rod-like shape. Some needle-like geometries are additionally observed. EDX analysis shows, as previously, stoichiometries of the M_7C_3 type.

Figure 6(a) presents the microstructure of the alloy after 180 min at 800 °C. Not any significant difference to the microstructure after 30 min of destabilization treatment at the same temperature can be observed; partial transformation of the austenitic dendrites into martensite has taken place. SEM examination (Fig. 6b) also reveals the presence of finely dispersed plate-like secondary carbide precipitates. Their morphological features, as mentioned earlier, indicate $M_{23}C_6$ stoichiometries. However, morphological modifications of isolated precipitates to rod-like shapes are discerned that possibly indicate transformation from $M_{23}C_6$ to M_7C_3 stoichiometries.

Increasing the destabilization temperature to 900 °C has led to a full transformation of the austenitic islands to martensite, as illustrated in Fig. 7(a). SEM examination (Fig. 7b) reveals the presence of secondary carbide precipitates of mixed-plate and rod like-morphology. After 180 min at 1000 °C, the austenitic dendrites have completely been transformed to martensite; an extensive secondary carbide precipitation is also noticed. However, a slight increase in the austenitic phase within the eutectic constituent along with eutectic carbide coarsening can

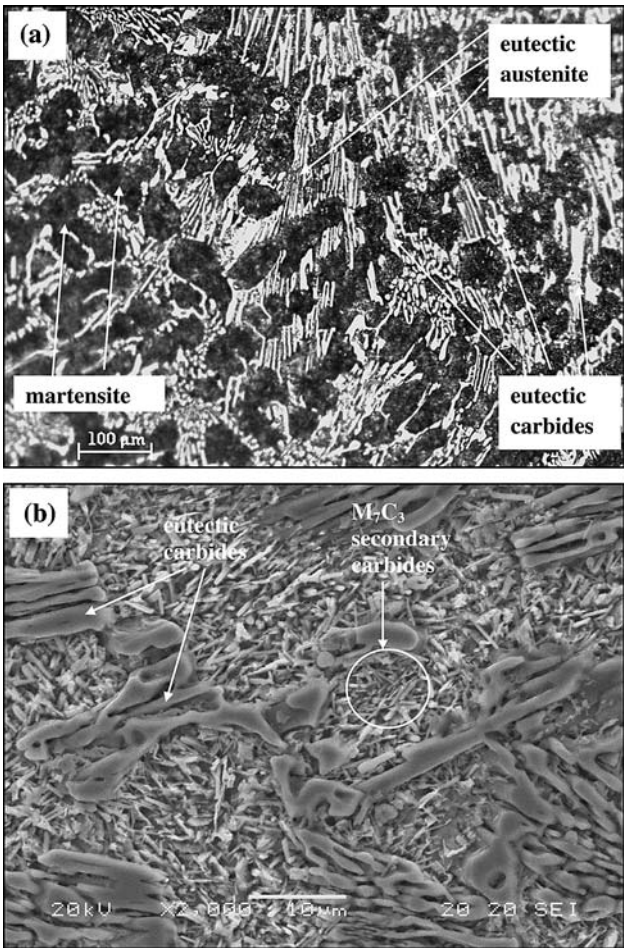

Fig. 5 Destabilization at 1100 °C for 30 min. (a) Eutectic carbides, martensite, and increased extent of eutectic austenite. The brighter contrast of the martensite islands, in comparison with that of Fig. 3, is due to extensive carbide precipitation. (b) Extensive precipitation of needle/rod-like M_7C_3 secondary carbides

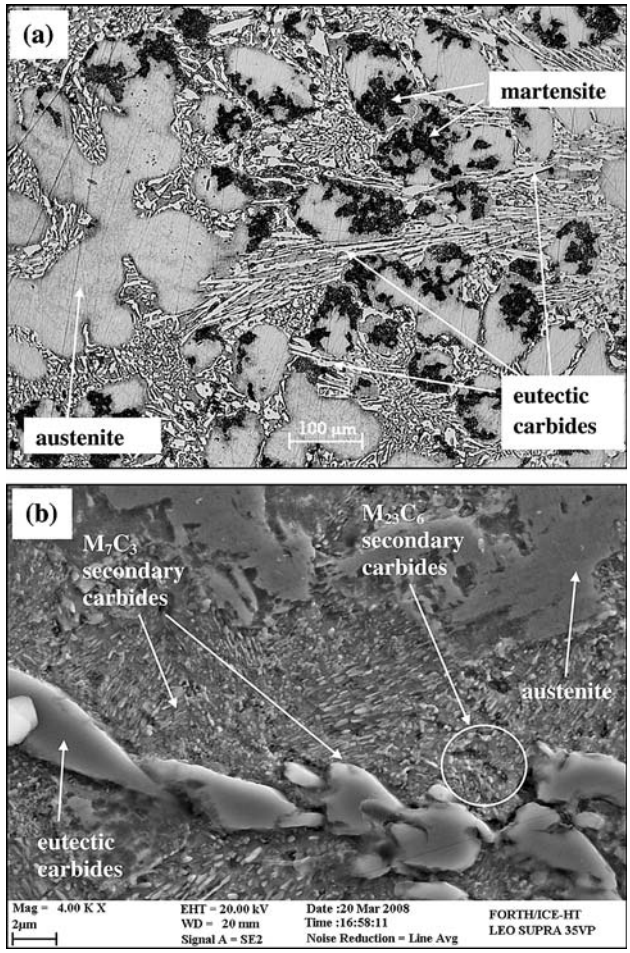

Fig. 6 Destabilization at 800 °C for 180 min. (a) Eutectic carbides/austenite and austenitic dendrites partially transformed to martensite. (b) Extensive plate-like secondary carbide precipitation of $M_{23}C_6$ stoichiometry. Areas of M_7C_3 formation are also observed

be discerned (Fig. 8a). SEM examination (Fig. 8b) reveals extensive secondary carbide precipitation of needle- and rod-like morphology and M_7C_3 stoichiometry (according to EDX analysis). A slight coarsening of the secondary carbide particles can be observed.

Figure 9(a) presents the microstructure of the alloy after destabilization at 1100 °C for 180 min. An increase in the austenitic phase, especially at the eutectic constituent, and coarsening of the eutectic carbide phase is noticed. SEM examination (Fig. 9b) reveals the presence of coarse secondary carbide particles of rod-like shape and M_7C_3 stoichiometry (the latter determined by EDX), as well as the presence of austenite.

3.2.3 Effect of Destabilization Time on the Microstructure. To elaborate the effect of destabilization time on the alloy microstructure, three different times were selected: 30, 210, and 240 min for each one of the temperatures: 800, 1000, and 1100 °C.

Figure 10 shows the microstructure of the destabilized alloy after treatment at 800 °C for 210 min (Fig. 10a) and 240 min (Fig. 10b). Comparing these microstructures with the microstructure at 800 °C for 30 min (Fig. 2b), an increase in the amount of the plate-like secondary precipitates can be observed, which is more intensive at the prolonged times. Localized areas of $M_{23}C_6$ to M_7C_3 transformation initiation can be discerned.

Figure 11(a) and (b) present the microstructures of the destabilized alloy, after been treated at 1000 °C for 210 and 240 min, respectively. Clearly an increase in the amount and size of the secondary carbide precipitates is noticed, as compared to the microstructure of the alloy at the same temperature for 30 min (Fig. 4b). The needle- and rod-like M_7C_3 secondary precipitates appear coarser, especially after 240 min of treatment. For both these prolonged treatments, the secondary carbides appear to grow with a pattern that resembles the Widmanstätten structure.

The microstructures of the destabilized material after heat treatment at 1100 °C for 210 and 240 min are illustrated in Fig. 12(a) and (b), respectively. A profound change is noticed in comparison with the structure obtained after 30 min at the same temperature (Fig. 5b). The vast majority of the secondary carbide precipitates have dissolved into the austenitic matrix, which, after this dissolution process, is enriched in alloying elements and, thus, more stable; this stability has resulted in its retention during the cooling stage. The porous-like texture of the austenitic phase indicates its unsuccessful attempt to transform to martensite, since the martensitic transformation is accompanied by volume expansion.

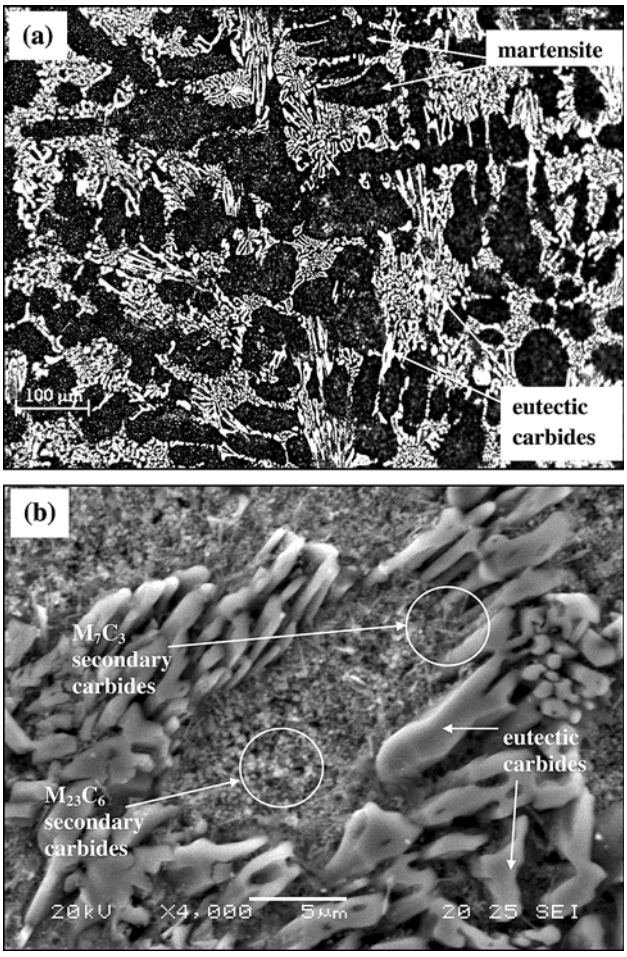

Fig. 7 Destabilization at 900 °C for 180 min. (a) Eutectic carbides and martensite. (b) Plate-like $M_{23}C_6$ secondary and M_7C_3 rod-like carbide particles

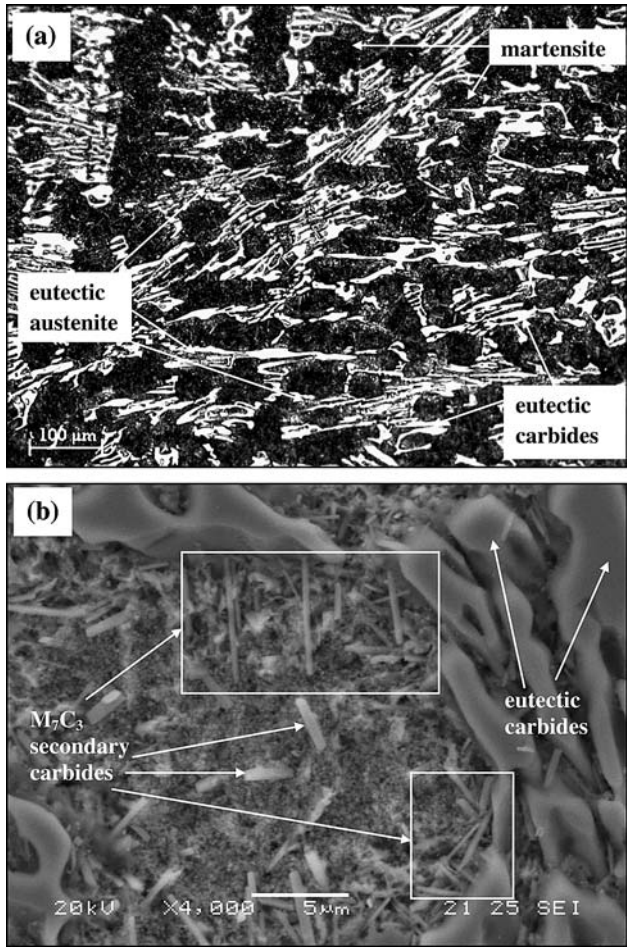

Fig. 8 Destabilization at 1000 °C for 180 min. (a) Eutectic carbides, martensite, and slight increase in the eutectic austenite phase. (b) Extensive precipitation of needle- and rod-like M_7C_3 secondary carbides

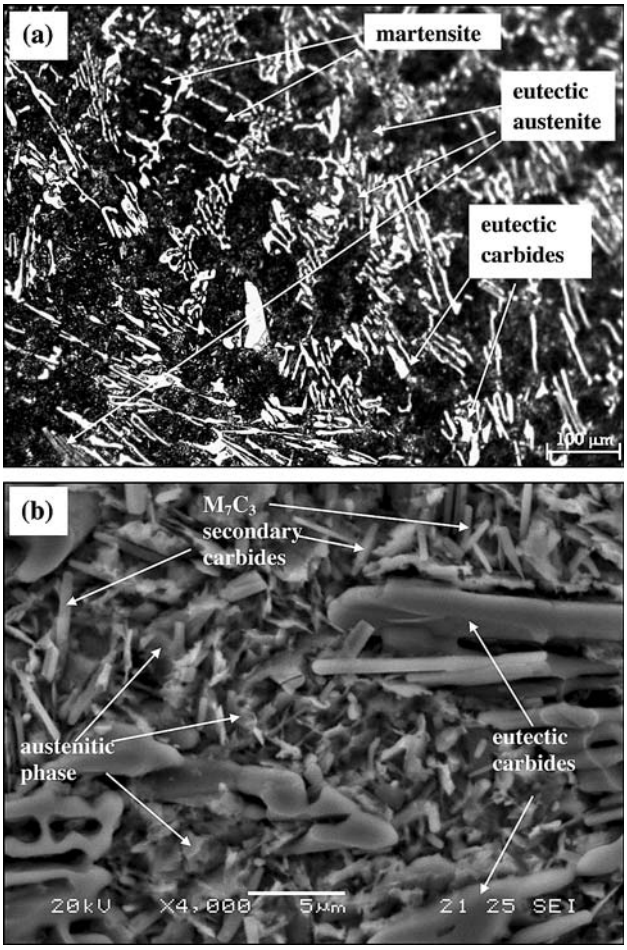

Fig. 9 Destabilization at 1100 °C for 180 min. (a) Eutectic carbides, martensite, and increased extent of eutectic austenite. (b) Extensive precipitation of needle/rod-like M_7C_3 secondary carbides

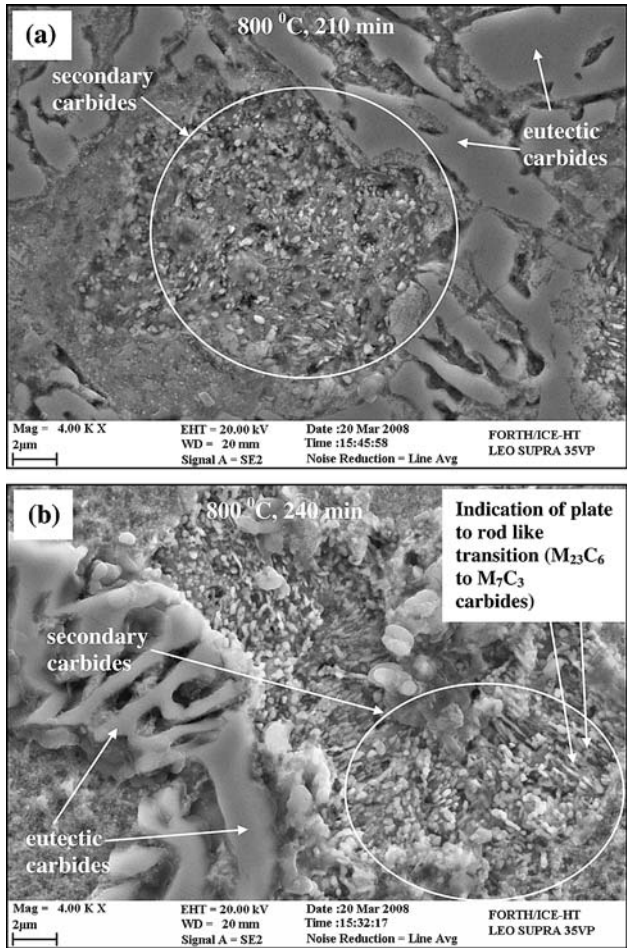

Fig. 10 Microstructures received after destabilization at 800 °C for: (a) 210 min, showing extensive precipitation of plate-like $M_{23}C_6$ secondary carbide particles and localized formation of (and/or transformation to) M_7C_3 secondary carbides, and (b) 240 min, showing similar microstructural features

3.2.4 Correlation of Microstructure and Hardness. At 800 °C, a continuous increase in the alloy bulk hardness versus time occurs (Fig. 1). On the basis of the respective microstructures (Fig. 2 and 9a, b), this increase is mostly associated with the continuous precipitation of $M_{23}C_6$ plate-like particles within the bulk alloy along with the consequent transformation of the austenitic matrix to martensite. At 900 °C, a rapid increase in hardness versus time is observed for short destabilization times. These phenomena are in agreement with other experimental efforts (Ref 20) and indicate that the precipitation of secondary carbide phases is more intensive at the early stages of the destabilization process. Hardness eventually reaches a plateau, where the amount, shape/morphology, and stoichiometry of the secondary carbides along with the extent of martensitic formation have achieved an optimum combination (regarding hardness) for the temperature of 900 °C. Similar behaviors are observed for destabilization at 1000 and 1100 °C. An additional hardening mechanism at these two temperatures is the growth of needle- and rod-like M_7C_3 particles with a Widmanstätten-like pattern. The highest hardness values are obtained after destabilization at 1000 °C, suggesting that the best combination of the afore-mentioned morphological features has been achieved. The dissolution of the secondary carbides and the subsequent stabilization of the austenitic phase at 1100 °C are responsible for the lower hardness values, as compared to those at 900 and 1000 °C. However, the presence of some carbide precipitates and martensitic phase lead to hardness values higher than those at 800 °C. The slight decrease in the hardness of the alloys subjected to prolonged destabilization at 900, 1000, and 1100 °C can be attributed to carbide particle coarsening (1000 °C) and dissolution to the austenitic matrix (1100 °C). The general behavior of the alloys regarding hardness is in agreement with the findings of Jacuinde-Bedolla et al. (Ref 20), despite the shifting of the temperature where the maximum values are obtained toward lower values; this shift is possibly associated with compositional differences of the examined alloys.

4. Conclusions

The present work investigates the effect of destabilization time and temperature on the microstructure and hardness of a 18.22 wt.% Cr white iron. The main conclusions drawn are:

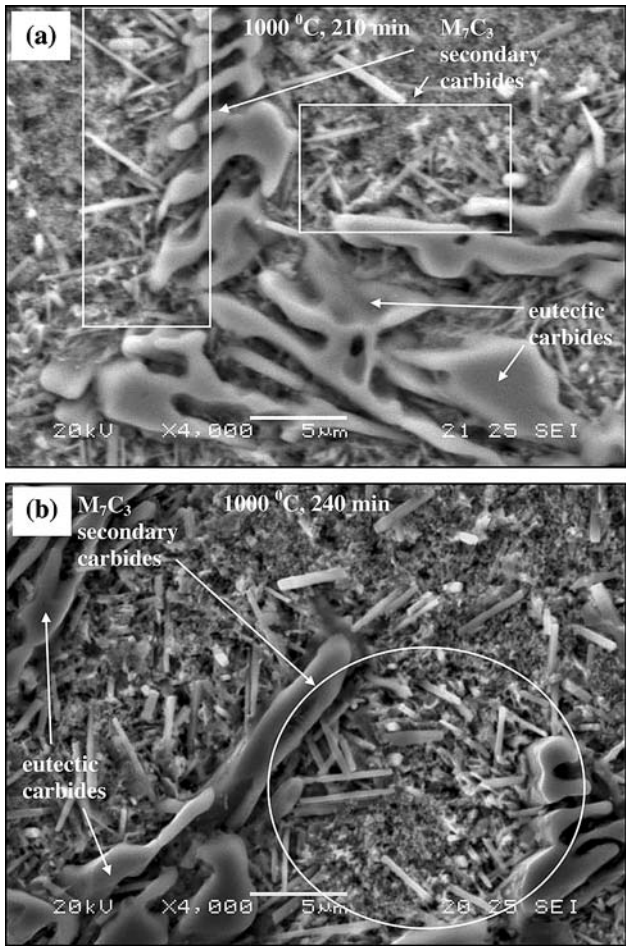

Fig. 11 Microstructures received after destabilization at 1000 °C for: (a) 210 min, showing extensive precipitation of needle/rod-like M_7C_3 secondary carbide particles, and (b) 240 min, showing similar microstructural features. In both cases, the secondary carbide particles form a similar to Widmastätten morphology

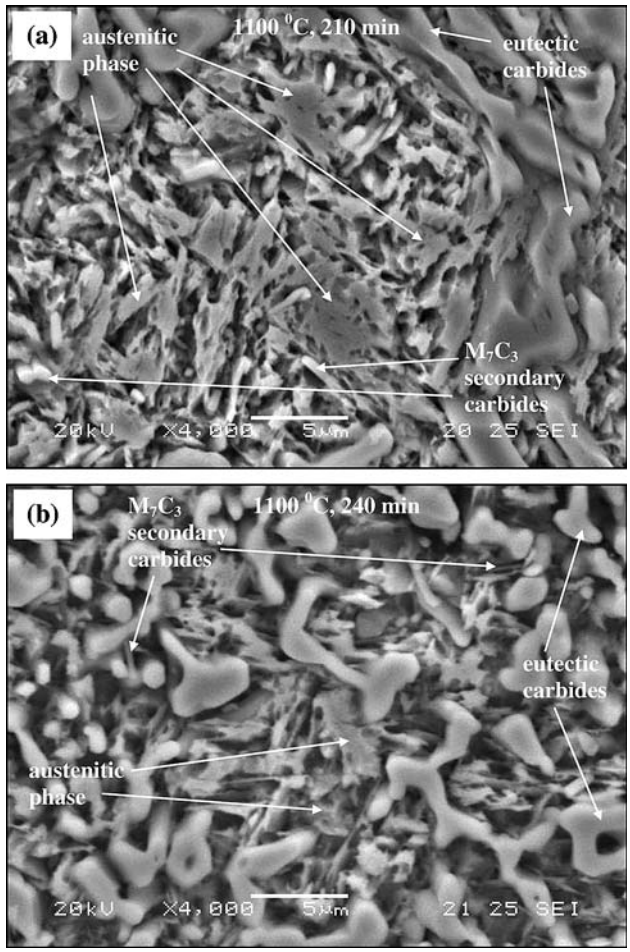

Fig. 12 Microstructures received after destabilization at 1100 °C for: (a) 210 min, showing extensive formation of austenitic phase and some precipitation of rod-like M_7C_3 secondary carbide particles, and (b) 240 min, showing an almost complete absence of the secondary carbide precipitates

1. Destabilization at 800 °C leads to precipitation of plate-like secondary $M_{23}C_6$ particles gradually progressing with time; as a result, a gradual increase in the alloy bulk hardness with time occurs. The austenitic matrix is partially transformed to martensite.
2. During destabilization at 900 °C, an initial sharp increase in the bulk hardness is observed, due to both secondary carbide particle precipitation, of mainly plate-like morphology, and matrix transformation to martensite. Then, a gradual reduction in the rate of hardness increase occurs, followed by a stabilization trend, owing to further carbide precipitation of the M_7C_3 type and coarsening phenomena. The latter becomes intensive at the longest destabilization times, leading to a slight decrease in the alloy hardness.
3. The same trend in hardness is observed for destabilization at 1000 °C; the maximum values of hardness are obtained at this temperature, due to the optimum combination of carbide precipitation, carbide particle morphology, as well as extent of martensite formed.
4. At 1100 °C, dissolution of carbides takes place, leading to stabilization of the austenitic phase. These phenomena are responsible for the hardness decrease to values lower than those achieved at 900 and 1000 °C.

Acknowledgments

The authors would like to acknowledge the Greek Modern Castings (GMC) S.A foundry for their kind assistance in the preparation of the examined alloy. They would also like to acknowledge, Dr. Vassilios Drakopoulos, Principal Scientist of the Institute of Chemical Engineering and High Temperature Process of the Foundation of Research, Greece and Mr. Alexander Katsoulidis, Post-graduate student of the Chemistry Department of the University of Ioannina, Greece for their assistance in the SEM examination.

References

1. C.P. Tabrett, I.R. Sare, and M.R. Ghomashchi, Microstructure-Property Relationships in High Chromium White Iron Alloys, *Int. Mater. Rev.*, 1996, **41**(2), p 52–89
2. C.P Tabrett and I.R. Sare, The Effect of Heat Treatment on the Abrasion Resistance of Alloy White Irons, *Wear*, 1997, **203–204**, p 206–219
3. C.P. Tabrett and I.R. Sare, Effect of High Temperature and Sub-Ambient Treatments on the Matrix Structure and Abrasion Resistance of a High Chromium White Iron, *Scr. Mater.*, 1998, **38**(12), p 1747–1753

4. O.N. Dogan, J.A. Hawk, and G. Laird II, Solidification Structure and Abrasion Resistance of High Chromium White Irons, *Metall. Mater. Trans.*, 1997, **28A**, p 1315–1328
5. O.N. Dogan and J.A. Hawk, Effect of Carbide Orientation on Abrasion of High Cr White Cast Iron, *Wear*, 1995, **189**, p 136–142
6. O.N. Dogan, G. Laird II, and J.A. Hawk, Abrasion Resistance of the Columnar Zone in High Cr White Cast Irons, *Wear*, 1995, **181–183**, p 342–349
7. S. Turenne, F. Lavallee, and J. Masounave, Matrix Microstructure Effect in the Abrasion Resistance of High Chromium White Cast Iron, *J. Mater. Sci.*, 1989, **24**, p 3021–3028
8. M. Durand-Charre, *Microstructure of Steels and Cast Irons*, Springer-Verlag, New York, 2004, p 51–73, ISBN-13:9783540209638
9. C.P. Tabrett and I.R. Sare, Fracture Toughness of High-Chromium White Irons: Influence of Cast Structure, *J. Mater. Sci.*, 2000, **35**, p 2069–2077
10. J. Asensio, J.A. Pero-Sanz, and J.I. Verdeja, Microstructure Selection Criteria for Cast Irons with More Than 10 wt% Chromium for Wear Applications, *Mater. Character.*, 2003, **49**, p 83–93
11. G.L.F. Powell and G. Laird II, Structure, Nucleation, Growth and Morphology of Secondary Carbides in High Chromium and Cr-Ni White Irons, *J. Mater. Sci.*, 1992, **27**, p 29–35
12. A. Wiengmoon, T. Chairuangsri, A. Brown, R. Brydson, D.V. Edmonds, and J.T.H. Pearce, Microstructural and Crystallographical Study of Carbides in 30 wt% Cr Cast Irons, *Acta Mater.*, 2005, **53**, p 4143–4154
13. G.L.F. Powell and J.V. Bee, Secondary Carbide Precipitation in an 18 wt% Cr-1 wt% Mo White Iron, *J. Mater. Sci.*, 1996, **31**, p 707–711
14. S.D. Carpenter, D. Carpenter, and J.T.H. Pearce, XRD and Electron Microscope Study of a Heat Treated 26.6% Chromium White Iron Microstructure, *Mater. Chem. Phys.*, 2007, **101**, p 49–55
15. J. Wang, C. Li, H. Liu, H. Yang, B. Shen, S. Gao, and S. Huang, The Precipitation and Transformation of Secondary Carbides in a High Chromium Cast Iron, *Mater. Character.*, 2006, **56**, p 73–78
16. S.D. Carpenter and D. Carpenter, X-Ray Study of M_7C_3 Carbide within a High Chromium White Iron, *Mater. Lett.*, 2003, **57**, p 4456–4459
17. J.T.H. Pearce and D.W.L. Elwell, Duplex Nature of Eutectic Carbides in Heat Treated 30% Chromium Cast Iron, *J. Mater. Sci. Lett.*, 1986, **5**, p 1063–1064
18. J.T.H. Pearce, Examination of M_7C_3 Carbides in High Chromium Cast Iron Using Thin Foil Transmission Electron Microscopy, *J. Mater. Sci. Lett.*, 1983, **2**, p 428–432
19. A. Inoque and T. Masumoto, Carbide Reactions ($M_3C \Rightarrow M_7C_3 \Rightarrow M_{23}C_6 \Rightarrow M_6C$) During Tempering of Rapidly Solidified High Carbon Cr-W and Cr-Mo steels, *Metall. Trans.*, 1980, **11A**, p 739–747
20. A. Bedolla-Jacuinde, L. Arias, and B. Hernández, Kinetics of Secondary Carbide Precipitation in a High-Chromium White Iron, *J. Mater. Eng. Perform.*, 2003, **12**(4), p 371–382
21. A.E. Karantzalis, A. Lekatou, and H. Mavros, Microstructural Modifications of As-Cast High Chromium White Iron by Heat Treatment, *J. Mater. Eng. Perform.*, in press (doi:10.1007/s11665-008-9285-6)